IP- OOP interaction in the URM infilled frame structures: a new macro-modelling proposal

Bharat Pradhan, Liborio Cavaleri

University of Palermo, Department of Engineering, Viale delle Scienze-90128, Palermo, Italy

Abstract

Infilled frame structures with unreinforced masonry (URM) infills is a common construction practice all over the world. To correctly assess the seismic performance of these structures, the analysis of the behaviour of masonry infills under in-plane (IP) and out-of-plane (OOP) loading, as well as their interaction, is of primary importance. Different approaches are available in the literature with different level of approximation for the prediction of the IP-OOP infill behavior that state an increasing interest in this field. In this context, this paper presents a new macro-element model which is able to simulate the behaviour of URM infill walls under seismic IP and OOP actions. The model is the evolution of an approach having a 4 struts configuration characterized by one horizontal strut, one vertical strut and two diagonal struts representing the infill wall. The struts are modelled by fiber section beam-column elements and their compressive behavior is defined by empirical strength and strain parameters. The paper also presents the empirical equations to obtain empirical parameters based on mechanical properties of infill wall. Further, the validation of the proposed model with the experimental results available in the literature is discussed. Through the paper, the improved capacity to simulate arching mechanism in the infill walls under the action of OOP load and a better reliability in capturing the interaction effects between the IP and OOP actions are described.

Keywords: URM infill, macro model, In-plane (IP) and out of plane (OOP) interaction

1. Introduction

Infilled frame structures with unreinforced masonry (URM) infills is a common construction practice all over the world. Recent earthquakes have shown that such buildings' performance is strongly associated with the behavior of the URM infill walls. The observed damage types in these types of infill walls are mostly classified as either in-plane (IP) or out-of-plane (OOP) damage, although the

damage mechanisms are usually a combination of both IP and OOP. Experimental studies have been carried out in order to characterize the OOP performance of the URM infill walls considering previous IP damage [1-5]. Experiments have also been conducted to understand the influence of prior OOP damage in the IP behaviour of the infill walls [6-7]. However, IP loading followed by OOP loading is more common among experiments since it is more critical in the seismic performance of infilled frame structures. These studies have demonstrated that OOP capacity of the URM walls reduce with the increasing IP demands, and it is important to consider the IP-OOP behaviour and their interactions in the numerical modelling. More recently, experiments by Ricci et al. [8] and De Risi et al. [9] have also highlighted the need of considering the previous IP damage when estimating the OOP capacity of the URM infill wall.

Theoretical models and numerical techniques have been developed to account for the influence of infill walls on the overall response of infilled frame structure. The model of single equivalent diagonal strut has been the most popular and used first in the literature [10-19]. However, researchers have also found out that the use of single diagonal strut do not accurately addresses different aspects of the interaction between the frame and the infill and have proposed multiple diagonal struts instead to simulate the behaviour of masonry infills [20-26]. The concept of single equivalent diagonal strut have been extended to have reliable estimations of the stiffening effects of infill walls [27-28]. Similarly, inelastic behaviour of the equivalent diagonal strut under the action of monotonic loading was introduced to capture the nonlinear behaviour of the infilled frame [29-31]. Different techniques have been implemented in performing the cyclic analysis of infilled frame with the use of equivalent diagonal strut [32-35]. But, the concept of modelling the infill wall with an equivalent single or multiple struts remained limited to the representation of IP behaviour of the infill walls for long time.

The first model that could consider IP as well as OOP resistance of the infill wall under the action of combined IP and OOP load was given by Hashemi and Mosalam [36]. In this model, an infill wall is represented by a three dimensional strut-and-tie (SAT) model. The model has two diagonal struts

(one in each direction) and each of the two diagonal struts is modeled by four pin-connected compression beam elements jointed by a tension tie, common to both diagonal struts (Fig 1).

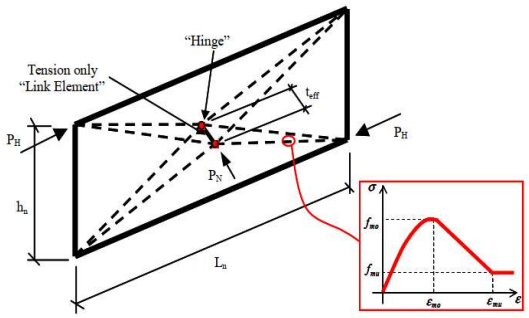

Fig 1 Strut and Tie model

(Hasehemi and Mosalam, 2007)

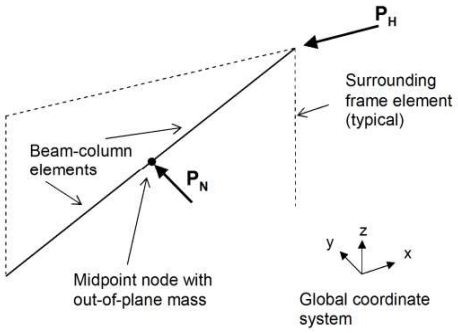

Fig 2 Macro-model for IP-OOP interaction

(Kadysiewski and Mosalam, 2009)

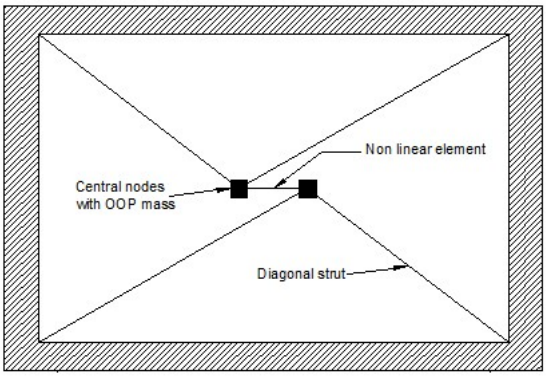

Fig 3 Macro model for IP-OOP interaction (Furtado et al., 2015)

Later, Kadysiewski and Mosalam [37] and Mosalam and Günay [38] proposed a single-strut model consisting of two fiber-section beam-column elements connected at the midpoint node with an assigned lumped mass (Fig 2) for the consideration of the response of the infill wall in the OOP direction. The diagonal strut is provided with both tensile and compressive characteristics. The cross-section of the beam-column element is modelled by locating nonlinear fibers along a line in the OOP direction. The calibration of the model is done at the fiber level by assigning different material properties to fibers at different locations in the cross section for the desired elliptical interaction of IP

and OOP load capacities. The macro model was developed in the open source software platform OpenSees [39].

Furtado et al. [40] proposed another simplified macro-model to simulate the IP and OOP behaviour of infill walls. The model is based on the approach of Rodrigues et al. [34] which was originally made to capture the IP behaviour of infill walls. In this model, each masonry infill wall is simulated by four diagonal struts with rigid behaviour and one central element where the non-linearity hysteresis is concentrated (Fig 3). To simulate the OOP behaviour, two central nodes with mass distributed equally to each node are introduced in the model. The model follows the element removal algorithm as in the model of Kadysiewski and Mosalam [37] and uses the trapezoidal IP-OOP interaction of load capacities to identify the damaged struts. Al Hanoun et al. [41] revalidated the concept of Furtado et al. [40] in the platform SAP 2000 [42] to identify the failure pattern and damage grades of primary (frame) and secondary elements(infill wall) of the RC frame structures.

All the aforementioned models are not straightforward, the calculation required is rigorous and are not easy to put into practical application. More recently, a four-strut macro element model was proposed by Di Trapani et al. [43] that can take in to account the IP and OOP behaviour of infill wall as well as their interaction (Fig 4). This macro model has two diagonal struts, one horizontal strut and one vertical strut. Each strut is represented by two fiber-section beam-column elements connected by a node at the mid-span. These 4 mid-span nodes can move independently in IP direction while they are constrained to move together in the OOP direction. In the model, the compressive behavior of the struts is defined by empirical strength and strain parameters. The use of fiber section elements to directly take into account the arching mechanism of infills during OOP load has been discussed in Asteresis et al. [44]. The accuracy of the model in simulating IP response is good but the model in some cases does not consider OOP response effectively. The other drawback of this model is the identification of the mechanical parameters to define the compressive behavior of the struts that is not based on a univocal procedure. Di Trapani et al. [45] have tried to establish a correlation based

approach to get the empirical parameters. However, the empirical equations are proposed to get the parameters for the IP analysis of the infilled frame.

In this paper, the macro-element model by Di Trapani et al. [43] has been modified to increase its accuracy in simulating both IP and OOP responses of the URM infill wall. The modified macro model retains similar 4 struts configuration, but has some major changes that makes this model simple and better. The proposed model has been validated with the experimental results. This paper also presents empirical equations to derive the empirical strength strain parameters which are required to define compressive behaviour of struts used in this macro model.

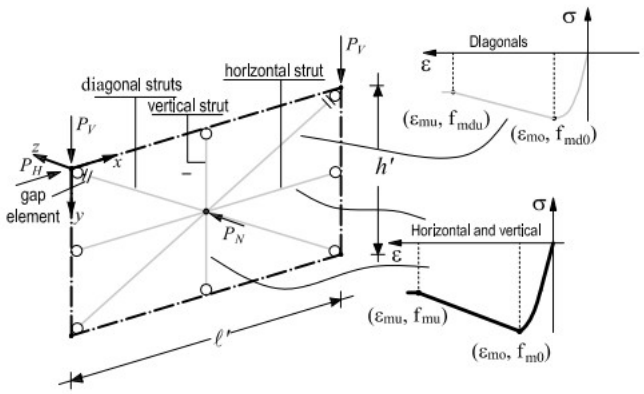

Fig 4 Four strut macro model by Di Trapani et al. (2018)

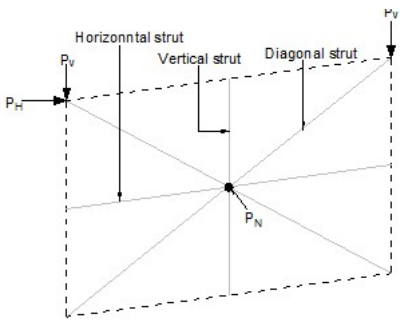

Fig 5 Proposed modified four strut macro model

2. Numerical modelling: Modified four strut macro model

The proposed model is a modification of the macro element model proposed by Di Trapani et al. [43]. The modified model retains its earlier 4 struts configuration i.e. there are two diagonal struts, one horizontal and one vertical strut. Each strut is represented by two beam-column elements connected by a node at the mid-span (Fig 5). These 4 mid-span nodes can move independently in IP direction while they are constrained to move together in the OOP direction. The macro model is formulated considering some basic requirements; the model has to account for the IP resistance of the infill wall, the model has to account for the arching mechanism under the action of OOP loads, the model has to account for the interaction between the IP and OOP actions and the model has to be simple to be used

in practice for seismic analysis of infilled frame structures. Some major changes made in the proposed modified macro model are as follows:

a. All the struts i.e. diagonals, vertical and horizontal struts, are transformed (rotated) so that all struts contribute more in OOP resistance, compared to transformation of only diagonal struts in the previous model.
b. All the struts are restrained against rotation at their connections with the frame rather than pin jointed to enable the struts to take into account the arch mechanism more effectively.
c. Single value of effective compressive strength is used for all struts rather than using the "effective" compressive strength for diagonal struts and actual compressive strength of infill wall for the horizontal and vertical strut.

In the model, the width of the diagonal struts 'w_d' is taken as one-third of the diagonal length 'd' while the width of the horizontal strut 'w_h' and vertical struts 'w_v' are calculated as a function of w_d, that is

$$w_d = \frac{d}{3} \;\; ; \;\; d = \sqrt{l'^2 + h'^2} \qquad [1a]$$

$$w_h = h - \frac{w_d}{\cos\theta} \qquad [1b]$$

$$w_v = l - \frac{w_d}{\sin\theta} \qquad [1c]$$

l and h are the clear length and height of the infill wall, respectively. l' indicates the centre to centre distance between the columns while h' indicates the distance from top of the lower beam to the centre of the top beam. The dimensioning of the struts are shown in Fig 6.

If 'w_d' is the width of the diagonal strut, '$w_d/\cos\theta$' is the total contact length between the diagonal struts and the columns and '$w_d/\sin\theta$' is the total contact length between with the diagonal struts and the beams. The thickness of all the struts are equal to the thickness of the infill wall. For simplicity, the thickness of the diagonal, vertical and horizontal struts are designated as 't'.

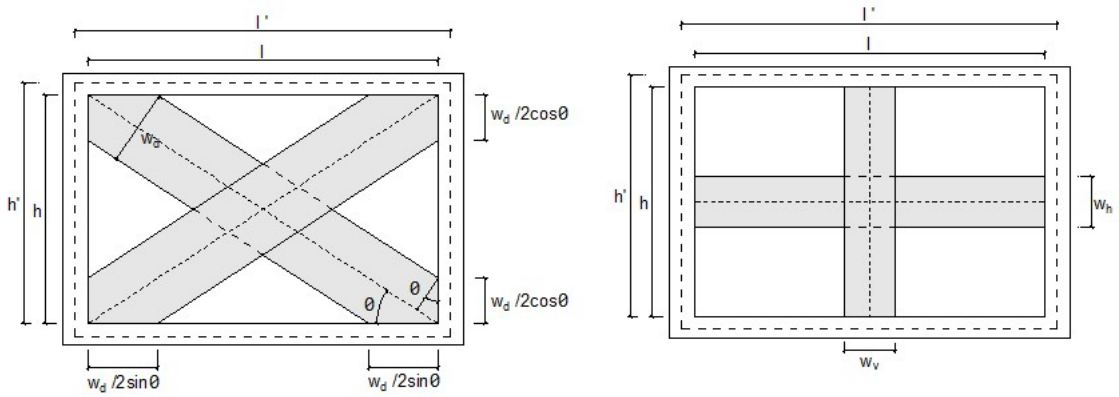

Fig 6 Dimensioning of the diagonal, vertical and horizontal struts

For a fiber-section beam element, the rate of internal force increment $\dot{s}^s(x)$ at a section can be related to the rate of increment of the section deformation, $\dot{e}^s(x)$ through the tangent stiffness matrix $k_T^s(x)$, by the following relation in Eq. 2.

$$\dot{s}^s(x) = \begin{bmatrix} \dot{N}(x) \\ \dot{M}(x) \end{bmatrix} = k_T^s(x) = \begin{bmatrix} \dot{\varepsilon}_0 \\ \dot{k} \end{bmatrix} = k_T^s(x)\dot{e}^s(x) \quad [2]$$

where $\dot{\varepsilon}_0$ is axial strain rate at centroidal axis of beam, $\dot{k}$ is the rate of change of section curvature, $\dot{N}(x)$ is the rate of change of axial force while $\dot{M}(x)$ is the rate of change of bending moment. After cracking in the fiber section, the change in the axial load and bending moment is related to the change in the axial strain and curvature as follows:

$$\dot{N}(x) = k_{T,11}^s \dot{\varepsilon}_0 + k_{T,12}^s \dot{k} \quad [3a]$$

$$\dot{M}(x) = k_{T,21}^s \dot{\varepsilon}_0 + k_{T,22}^s \dot{k} \quad [3b]$$

The section stiffness and resistance derives from the uniaxial stress–strain relation specified for each fiber in the section. The compressive behavior of masonry is represented by using an appropriate constitutive model for the strut elements. Kent–Park model [46] for concrete with the tensile strength equal to zero is chosen for this purpose (Fig 4). An update is made in this modified model regarding the use of compressive strength for the struts. In contrast to the previous provision of using the so-called effective compressive strength for the diagonal struts and the actual compressive strength of masonry for the vertical and horizontal struts, a single value of an effective compressive strength is adopted for all the struts evaluated by an approach different from that adopted for the previous

129 strategy, that was proved to be not always reliable. This provision has further simplified the model.
130 To represent the IP resistance, actual thickness of the infill can be applied for all struts and it yields
131 good numerical results. But, for the case of OOP resistance, the use of the actual infill thickness as a
132 strut thickness yields comparatively low strength. Hence, to accurately represent both the IP and OOP
133 resistances of the infill wall, the width and thickness of the all the diagonal, vertical and horizontal
134 struts are replaced by surrogate values that maintain the same cross-sectional area. The surrogate
135 values can be obtained with the following procedure.

136 To determine the surrogate width '$\tilde{w}$'and surrogate thickness '$\tilde{t}$' of the struts, it is assumed that the
137 OOP resistance of a strut 'q' is proportional to the compressive strength of the masonry 'f_m' and the
138 strut width 'w' and is inversely proportional to the square of the slenderness ratio 'l_s/t' of the strut as
139 follows (this procedure is also discussed in detail in Di Trapani et al. [43]):

140 $$q \propto \frac{f_m\, w}{\left(\frac{l_s}{t}\right)^2} \qquad [4]$$

141 In Eq. 4 'l_s' is the length of the strut. If f_m is to be replaced by f_{mo} to ensure the IP behavior is reliable
142 and the OOP resistance is to remain the same, the strut width 'w' and thickness 't' have to be replace
143 by '$\tilde{w}$' and '$\tilde{t}$', so that

144 $$\frac{f_m\, w}{\left(\frac{l_s}{t}\right)^2} = \frac{f_{m0}\tilde{w}}{\left(\frac{l_s}{\tilde{t}}\right)^2} \qquad [5]$$

145 To maintain the correct IP resistance, the cross-sectional area of the diagonal strut has to remain
146 unchanged, i.e. the area of the surrogate strut should be equal to the area of original strut.

147 $$w\, t = \tilde{w}\,\tilde{t} \qquad [6]$$

148 Substituting the expression for w from Eq. (6) into Eq. (5), one gets

149 $$\frac{f_m\, w}{\left(\frac{l_s}{t}\right)^2} = \frac{f_{m0}\, w\, t}{\tilde{t}\left(\frac{l_s}{\tilde{t}}\right)^2} \qquad [7]$$

On simplification and with relation to Eq. (6), the following relations for the surrogate width and thickness of the strut can be obtained:

$$\widetilde{w} = \frac{f_{mo}}{f_m}\, w \qquad [8a]$$

$$\tilde{t} = \frac{f_m}{f_{mo}}\, t \qquad [8b]$$

According to this procedure, the surrogate width and thickness of all the struts can be calculated if the compressive strength (f_m), the effective compressive strength (f_{mo}), and the original strut width (w) and thickness (t) are known. The surrogate width of diagonal, vertical and horizontal struts are represented by '$\widetilde{w}_d$', '$\widetilde{w}_v$' and '$\widetilde{w}_h$' respectively while the surrogate thickness for all struts is represented by $\tilde{t}$. The consideration of geometric nonlinearity in the model (in case of slender strut) is done by the use of beam-column elements formulated with the Corotational coordinate transformation. For hollow infill masonries, the properties like compressive strength 'f_m' and elastic modulus 'E_m' are usually not same in the direction of holes and perpendicular to the holes. The equivalent properties are derived by following the Eqs. 9:

$$f_m = \sqrt{f_{m1}.f_{m2}} \qquad [9a]$$

$$E_m = \sqrt{E_{m1}.E_{m2}} \qquad [9b]$$

The definition of f_m and E_m is purely conventional and this technique relates well with the equivalent strut stress–strain parameters to be used in the model. For the infill wall with solid masonry, the properties are considered equal in both vertical and horizontal directions.

3. Validation of the proposed macro model

The proposed model has been validated with some of the experimental data available in the literature. Angel [1] tested seven full-scale, single-story, single-bay RC infilled frames with both IP and OOP loads. The design details of the specimens are shown in Fig 7 while the geometric and material properties of the infills are given in Table 1. The specimens were first subjected to IP cyclic lateral

displacements until the infills reached double the drift of first cracking. The IP displacement history applied is shown in Fig 8, in which Δ_{cr} is the displacement at first cracking in the infills. Then the masonry infills were applied with monotonically increasing pressure in the OOP direction using an air bag. Specimens 2 and 3 which had the same infill thickness but different mortar properties subjected to IP drift of 0.34% and 0.22% respectively before applying OOP load are taken for the validation of the proposed model.

Numerical simulations were carried out in the software platform OpenSees. Frame elements as well as strut elements were modelled by fiber-section beam-column elements with distributed plasticity. Concrete 02 material model available in the numerical platform is used to simulate the behavior of the concrete and infill wall while reinforcement in the frames were simulated using Steel02 material model. Loading is applied in a similar pattern as used in the tests. The IP lateral displacement is applied at the upper nodes of the frame model and the OOP load is applied at the centre of the struts representing the infill centre. The geometrical and mechanical properties of the diagonal, vertical, and horizontal struts are presented in Tables 2 as determined.

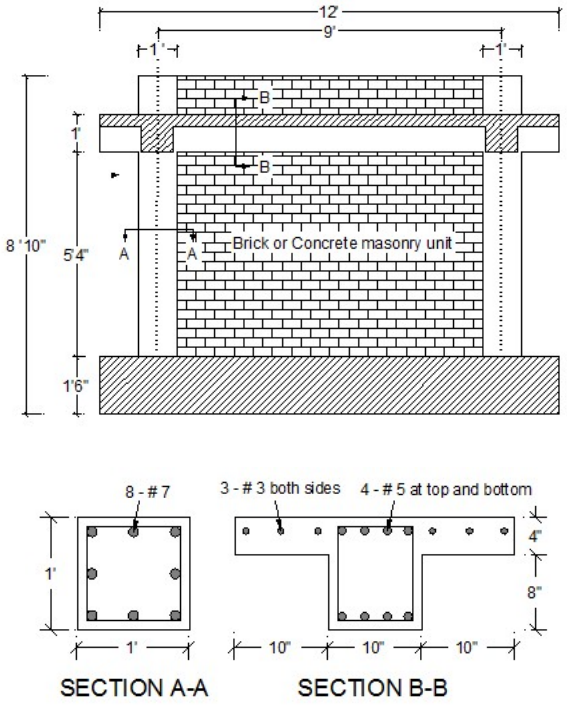

Fig 7 Details of Infilled frames tested by Angel (1994)

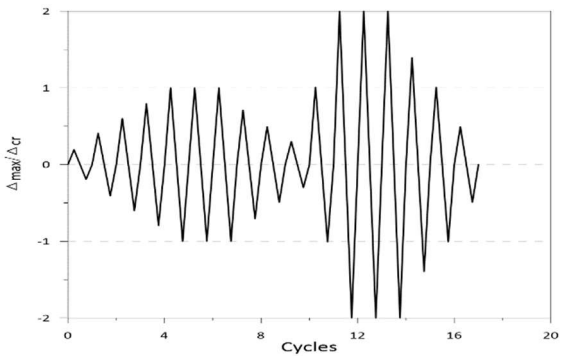

Fig 8 IP displacement history for Angel (1994)

Table 1 Geometrical and material properties of the masonry infills in Angel (1994)

Specimen	f_{m1} N/mm^2	f_{m2} N/mm^2	E_{m1} N/mm^2	E_{m2} N/mm^2	f_m N/mm^2	E_m N/mm^2	l mm	h mm	t mm	l' mm	h' mm	d mm
2	10.85	10.85	8040	8040	10.85	8040	2438.4	1625.6	47.6	2743.2	1782	3271.2
3	10.13	10.13	5212.4	5212.4	10.13	5212.4	2438.4	1625.6	47.6	2743.2	1782	3271.2

Table 2 Geometrical and mechanical properties of diagonal, vertical and horizontal struts calculated for Angel (1994)

Specimen	w_d mm	w_v mm	w_h mm	$\tilde{w}_d$ mm	$\tilde{w}_v$ mm	$\tilde{w}_h$ mm	t' mm	f_{mo} N/mm^2	f_{mu} N/mm^2	ε_{mo}	ε_{mu}
2	1090.4	472.6	315.1	261.3	113.3	75.5	198.6	2.6	1.56	0.0038	0.018
3	1090.4	472.6	315.1	387.5	168.0	112.0	133.9	3.6	2.16	0.0030	0.015

The material property of the strut fibers are defined by using 4 parameters, namely, f_{m0}, f_{mu}, ε_{mo} and ε_{mu}. These parameters are chosen in such a way that the numerical results match closely with the experimental results. The numerical results for the IP and OOP responses are shown in Fig 9 &10. The correlation between the experimental and the numerical results is reasonably good in spite of the simplicity of the model. The numerical results from the proposed model is also compared with the results from the earlier model given in Di Trapani et al. [43]. It can be observed that both the models yield similar IP response but the OOP response of the proposed modified model is more close to the experimental result. The improvement is better seen in the response for specimen 3. This verifies that the modified model accounts for OOP response comparatively better i.e. the proposed modifications enable the model to account for both IP and OOP responses of URM infill wall in a reliable way.

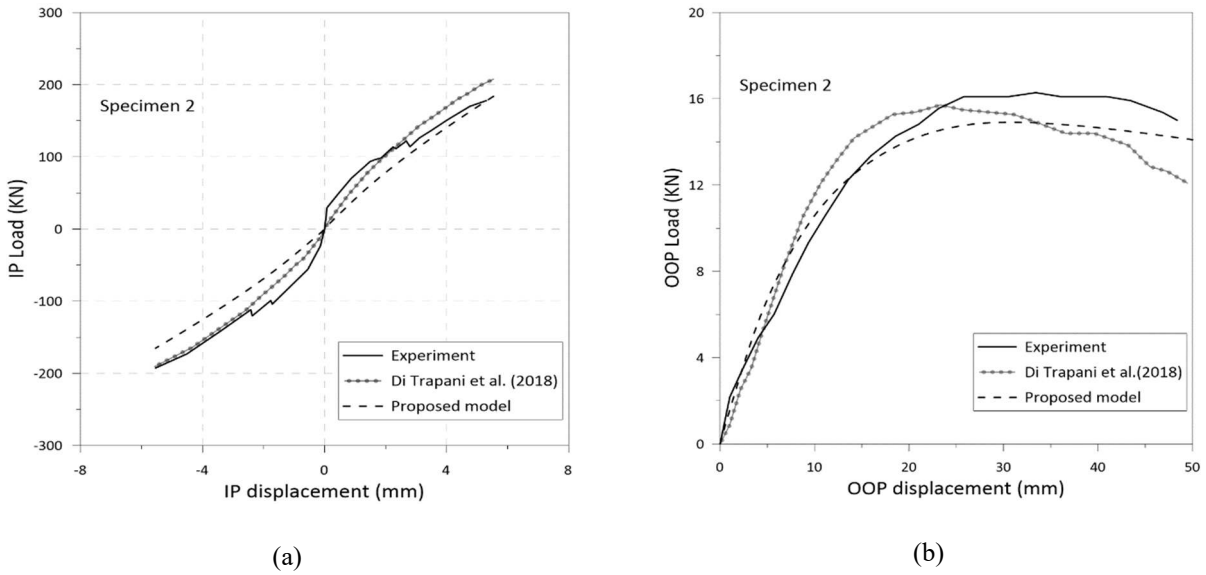

(a) (b)

Fig 9 Comparison of responses for specimen 2 of Angel (1994): a) IP responses; b) OOP responses

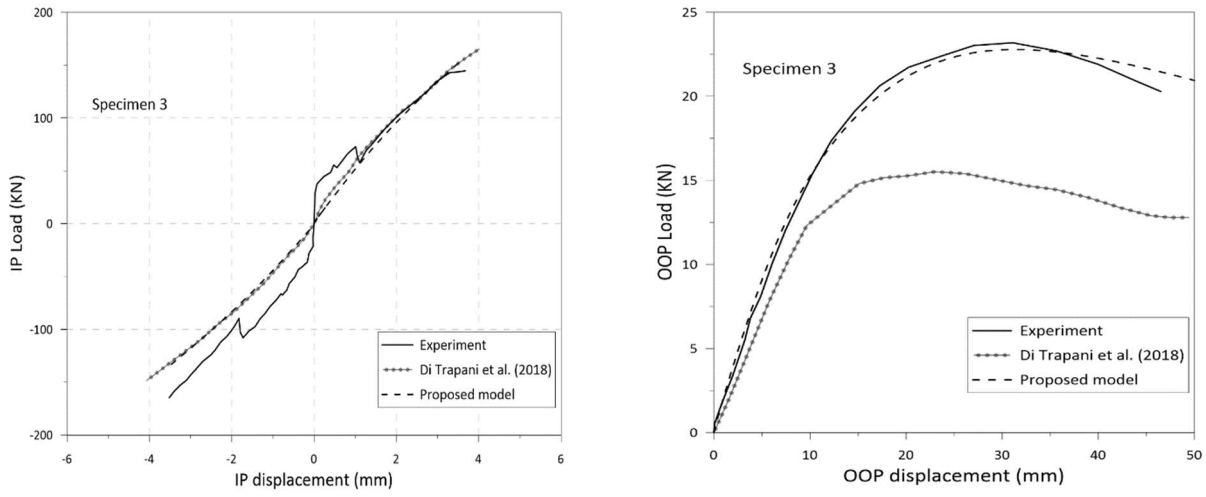

(a) (b)

Fig 10 Comparison of responses for specimen 3 of Angel (1994): a) IP responses; b) OOP responses

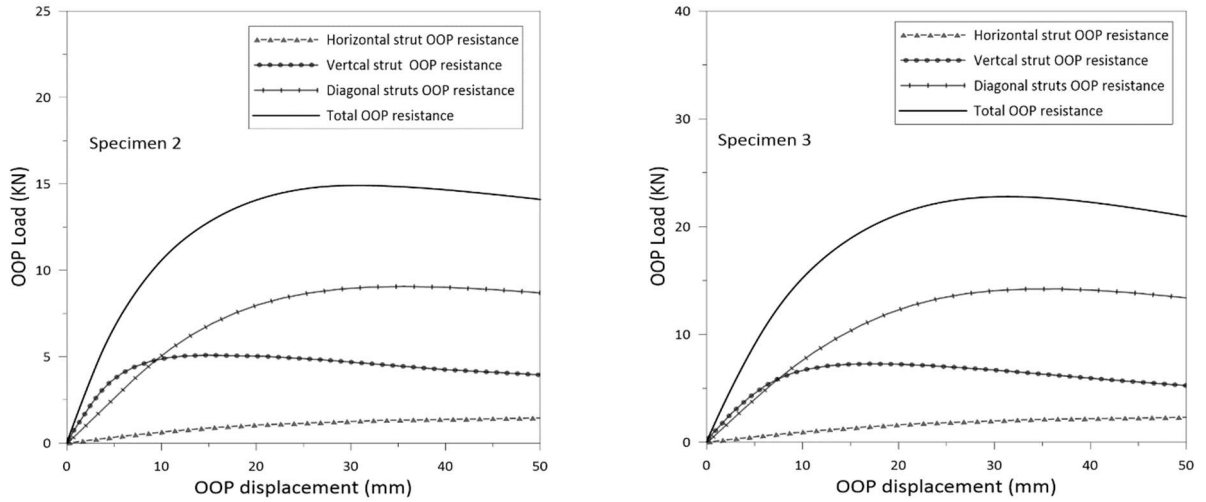

Fig 11 Role of horizontal, vertical and horizontal struts in OOP resistance for Angel (1994)

Fig 11 shows the role played by horizontal, vertical and diagonal struts separately in OOP resistance. According to the proposed model, diagonal and vertical struts offer bigger resistance while the horizontal strut has the least contribution in OOP resistance of infill wall.

The proposed model is further tested with other sets of experiments. The experimental studies which involves the cyclic IP loading at the top of infilled frame followed by monotonic OOP loading using the uniformly distributed load (air bag) or concentrated load (4 load points at the centre) on URM infill wall have been considered: Calvi & Bolognini [3]; Ricci et al. [8]; De Risi et al. [9]; Da Porto et al. [47]. Some other experiments which deals with IP and OOP load acting one after another to

213 determine the influence of prior IP damage on the response of URM infill wall like Flanagan &
214 Bennett [2], Pereira et al. [48], Hak et al. [49], Furtado et al. [50] have not be considered for numerical
215 simulation due to various reasons. For example, the experiment by Flanagan & Bennett [2] does not
216 provide the IP response of specimen subjected to IP load followed by OOP load (specimen 19).
217 Likewise, the experiment of Pereira [48] does not give details of the vertical load and the masonry
218 properties in two perpendicular directions for the infill wall made with hollow brick. The experiment
219 of Hak et al. [49] involved OOP loading –unloading- and reloading using a set of horizontal linear
220 points on the center of infill wall on both force and displacement controlled approach and this type
221 of OOP load is not better simulated numerically. Furtado et al. [50] tested single leaf wall in pure
222 OOP load and double leaf wall first in IP direction and then in OOP direction by removing the internal
223 leaf for comparison of the influence of previous IP damage. This feature of test involving the change
224 in the number of infill wythe or thickness during IP and OOP loading makes it difficult to simulate
225 numerically.

226 Calvi and Bolognini [3] tested an unreinforced infill panel with clay unit of thickness 135 mm. The
227 details of the tested infilled frame specimen is shown in Fig 12. The tests were performed under the
228 action of vertical loads applied on the columns. Infilled frame was subjected to two different IP drifts;
229 0.4 % (specimen 6) and 1.2 % (Specimen 2) and followed by OOP load applied monotonically on
230 four load points. Specimen 6 (#6) is taken for the numerical simulation by using the proposed model.
231 Da Porto et al. [47] tested RC frames infilled with URM walls made of up clay masonry units of
232 thickness 30 cm. The geometric details of the reference frame is shown in Fig 13. The experiment
233 was conducted in the presence of vertical load applied in each column. In-plane quasi static cyclic
234 horizontal displacement was imposed at the level of the top beam to a drift of 1.2 %. After the
235 application of cyclic in-plane drift, the infill panel was subjected to monotonic out-of-plane load at
236 four load points until collapse.

Ricci et al. [6] experimented two set of infill walls of thickness 80 mm (specimen #1) and 120 mm (specimen #2) to determine the influence of the slenderness ratio. Both of these specimens were tested for pure OOP load and also in IP load followed by OOP load. Specimens were subjected to three different level of IP drift before loading to OOP direction. IP tests were performed using quasi-static cycling loading at one end of the upper beam while OOP tests were performed using the four point loading method at the center of the infill.The details about the tested frame is show in Fig 14. For the numerical simulation, OOP response after the first level IP drift i.e. 0.16% for specimen #1 and 0.21% for specimen #2 is selected. De Risi et al. [9] continued the experimental campaign of Ricci et al. (2018) where the effect of the aspect ratio in OOP response of the infill was investigated. Infill wall of 80 mm thickness having an aspect ratio of 1:1 was tested in a similar fashion; a pure OOP test and OOP tests after each of three different IP drifts were carried out. The details of the frame is shown in Fig 15. For the numerical simulation, OOP response after 0.15% IP drift is taken. The IP drift history for all tests are shown in Fig 16. The material properties of the concrete frames and masonry infills are provided in Table 3 while the geometric properties of the masonry infills are given in Table 4.

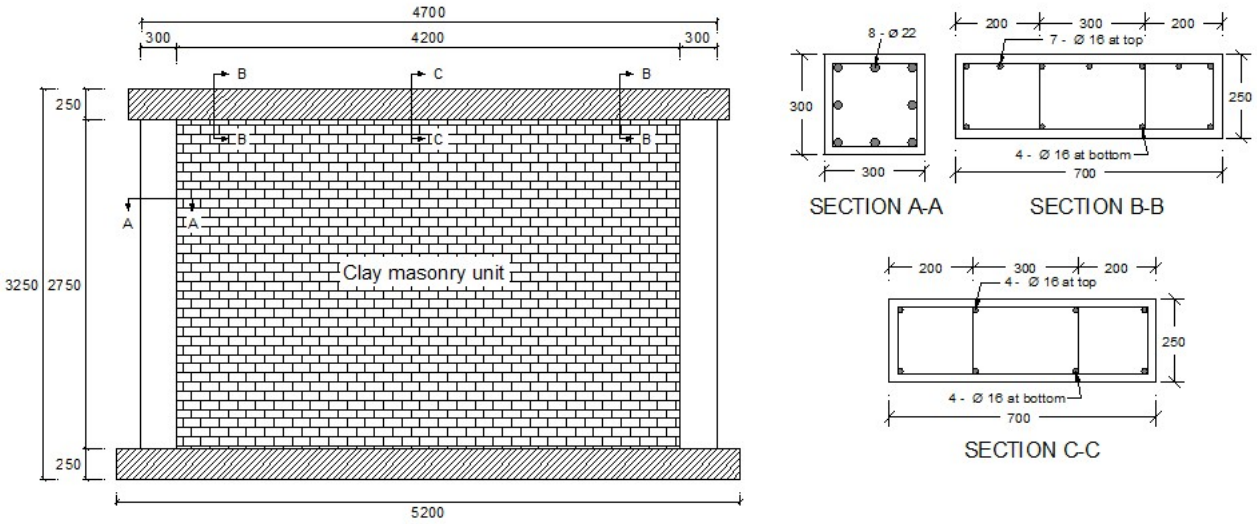

Fig 12 Details of the infilled frame tested by Calvi & Bolognini, 2001 (dimension in mm)

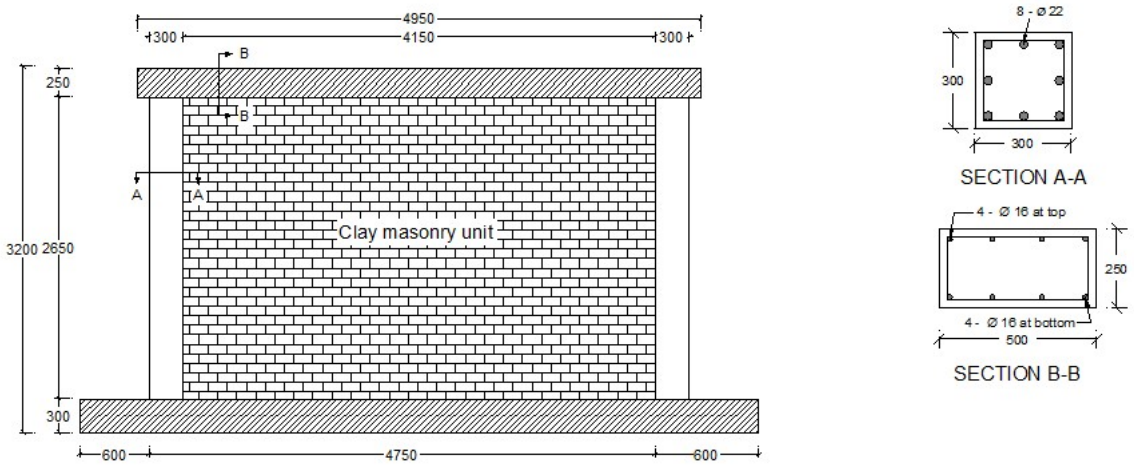

253 **Fig 13** Details of the infilled frame by tested by Da Porto et al., 2013 (dimension in mm)

254

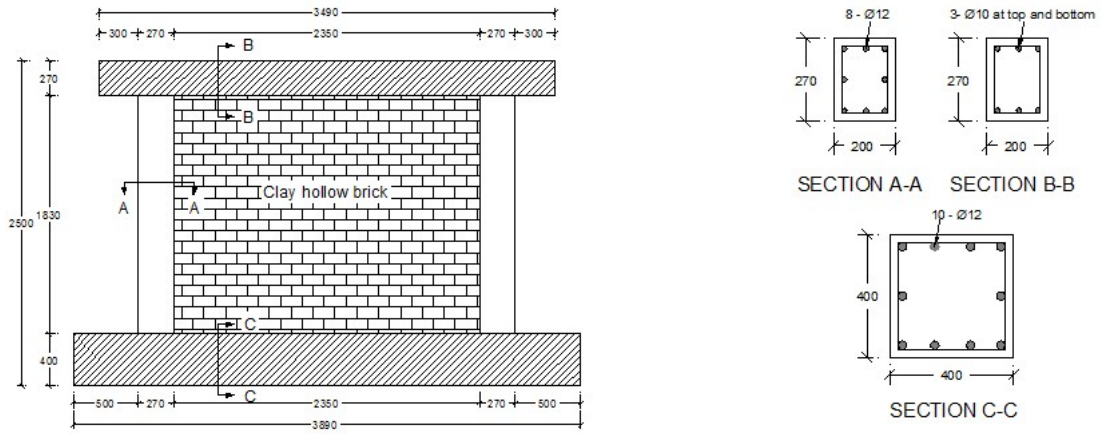

255 **Fig 14** Details of the infilled frame tested by Ricci et al., 2018 (dimension in mm)

256

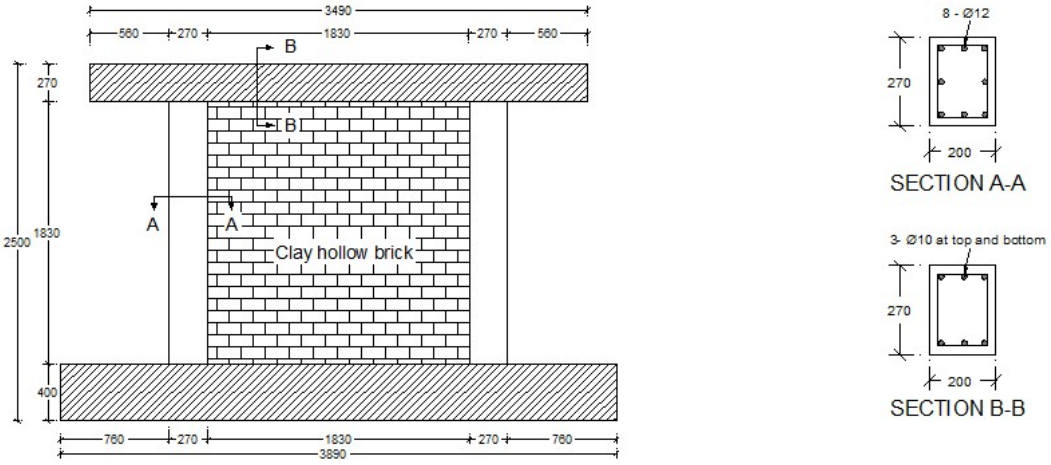

257 **Fig 15** Details of the infilled frame tested by De Risi et al., 2019 (dimension in mm)

258

Table 3 Material Properties of the Concrete Frame and Masonry Infills for Specimens under Study

Experiment		f_c N/mm^2	f_{m1} N/mm^2	f_{m2} N/mm^2	E_{m1} N/mm^2	E_{m2} N/mm^2	f_m N/mm^2	E_m N/mm^2
Calvi & Bolognini (2011)	#6	34.6	1.11	1.10	991	1873	1.105	1362.4
Da Porto et al. (2013)		36.4	6	1.19	4312	1767	2.67	2760.3
Ricci et al. (2018)	#1	36	2.45	1.81	1255	1090	2.11	1169.59
	#2	46.2	2.12	1.65	1262	1455	1.87	1355.07
De Risi et al. (2019)		42.9	4.63	2.37	3452	1891	3.31	2554.94

Table 4 Geometric Properties of the Masonry Infills Equivalent Struts for the Specimens under Study

Experiment		l mm	h mm	t mm	l' mm	h' mm	d mm	w_d mm	w_v mm	w_h mm
Calvi & Bolognini (2011)	#6	4200	2750	135	4500	2875	5510	1836.5	847.3	554.8
Da Porto et al. (2013)		4150	2650	300	4450	2775	5244	1748.1	901.8	575.8
Ricci et al. (2018)	#1	2350	1830	80	2620	1965	3275	1091.6	573.2	446.3
	#2	2350	1830	120	2620	1965	3275	1091.6	573.2	446.3
De Risi et al. (2019)		1830	1830	80	2100	1965	2876	958.6	474.2	474.2

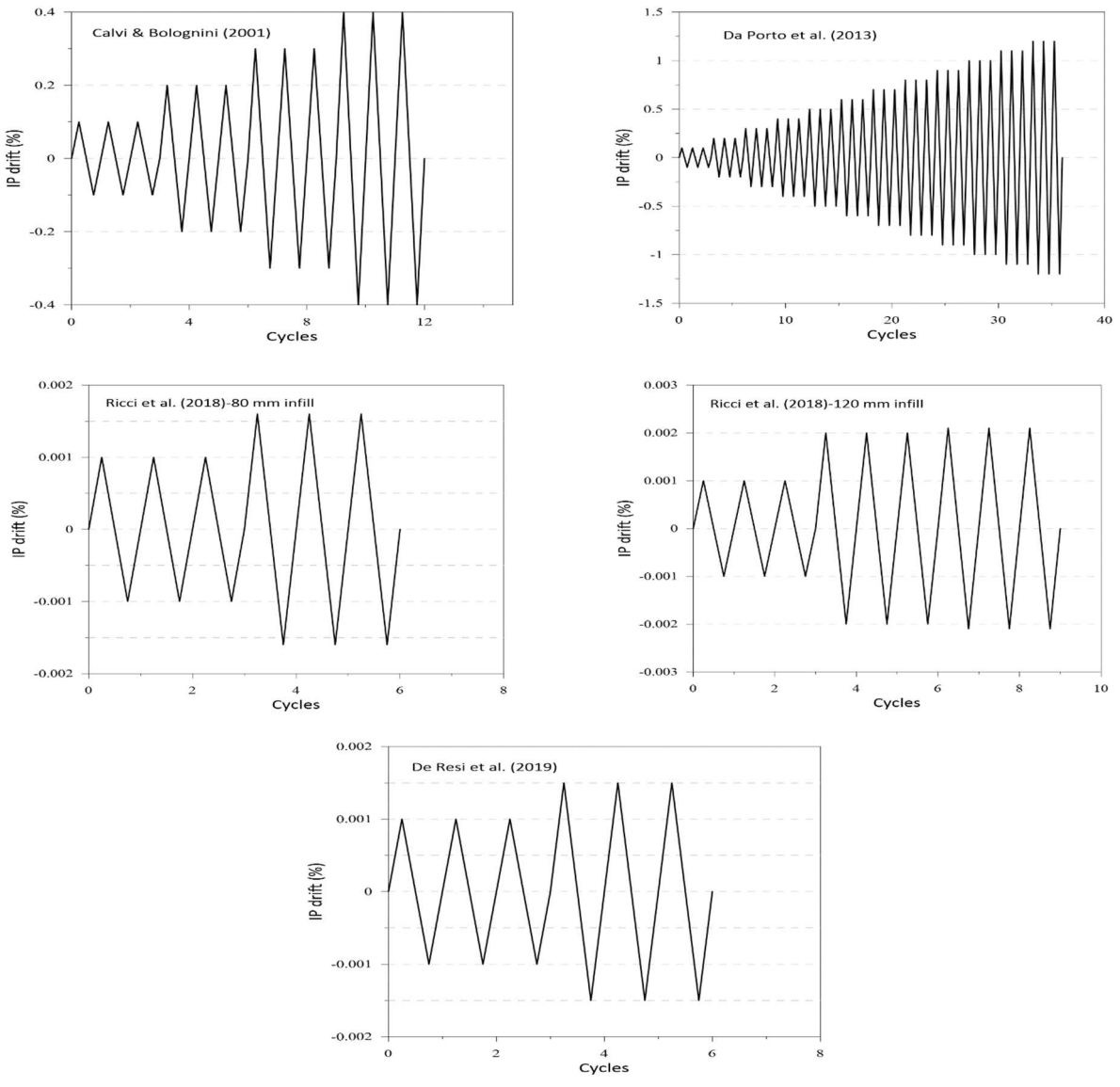

Fig 16 IP drift history applied during the experiment and numerical analysis

At first, numerical simulations were performed by assigning the strength strain parameters (f_{mo}, f_{mu}, ε_{mo}, ε_{mu}). The ultimate strength 'f_{mu}' was taken as 60% of the peak strength 'f_{mo}'. The simulations were performed assigning the mechanical characteristics in order to obtain responses similar to experimental results in both IP and OOP directions. Therefore, the parameters were fixed in such a way that the minimum offset was observed in both IP and OOP responses for all selected specimens under study. To this point a correlation was established between the effective mechanical parameters and the actual mechanical parameters of masonries. Finally, analyses were repeated by using the parameters calculated on the basis of the found correlations. The correlation between the infill properties will be discussed in the next section. The geometrical properties of the struts as well as the final effective parameters used for numerical analysis are listed in Table 5. The results obtained from the numerical simulations are shown in Fig 17-21.

Table 5 Geometrical and Mechanical Properties for the Diagonal, Vertical and Horizontal Struts

Experiment		$\widetilde{w}_d$ mm	$\widetilde{w}_v$ mm	$\widetilde{w}_h$ mm	$\tilde{t}$ mm	f_{mo} N/mm^2	f_{mu} N/mm^2	ε_{mo}	ε_{mu}
Calvi and Bolognini (2001)	#6	1259.8	581.3	380.6	196.8	0.758	0.45	0.00045	0.0053
Da Porto et al. (2013)		845.9	436.4	278.7	620.0	1.293	0.78	0.00069	0.0075
Ricci et al. (2018)	#1	440.6	231.4	180.2	198.2	0.851	0.51	0.00049	0.0057
	#2	500.2	262.7	204.5	261.9	0.857	0.51	0.00049	0.0057
De Risi et al. (2019)		400.5	198.1	198.1	191.5	1.384	0.83	0.00073	0.0079

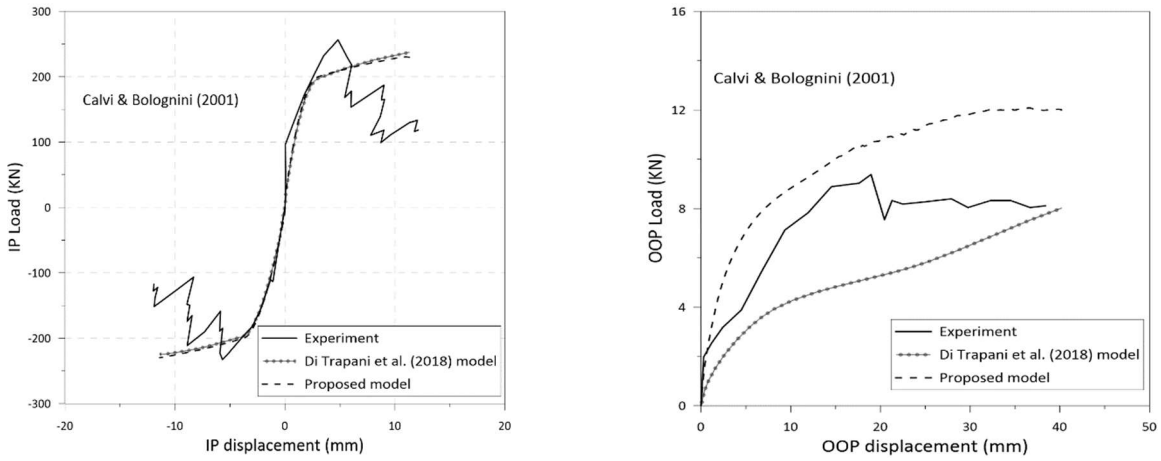

(a) (b)

Fig 17 Comparison of responses for specimen 6 of Calvi & Bolognini (2001): a) IP responses; b) OOP responses

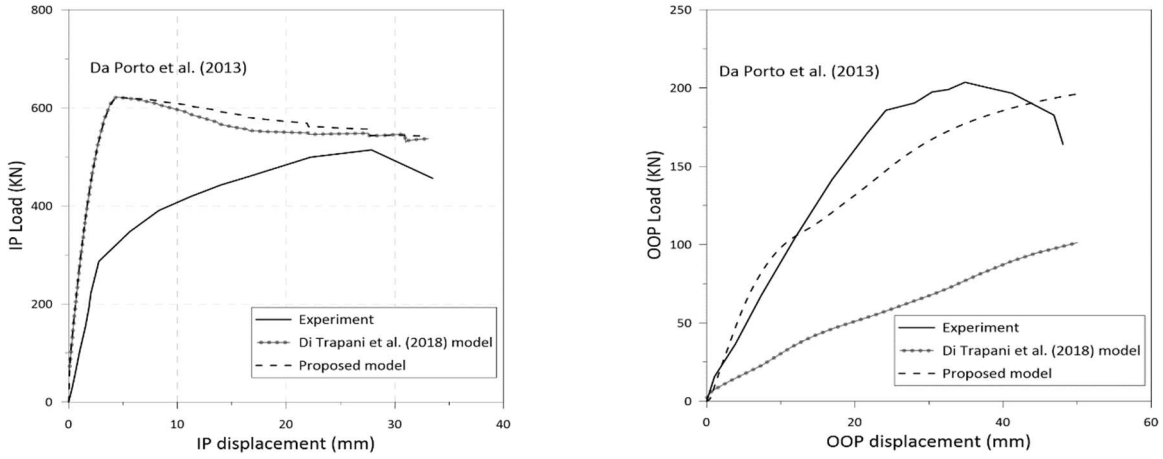

(a) (b)

278 **Fig 18** Comparison of responses for Da Porto et al. (2013): a) IP response; b) OOP response

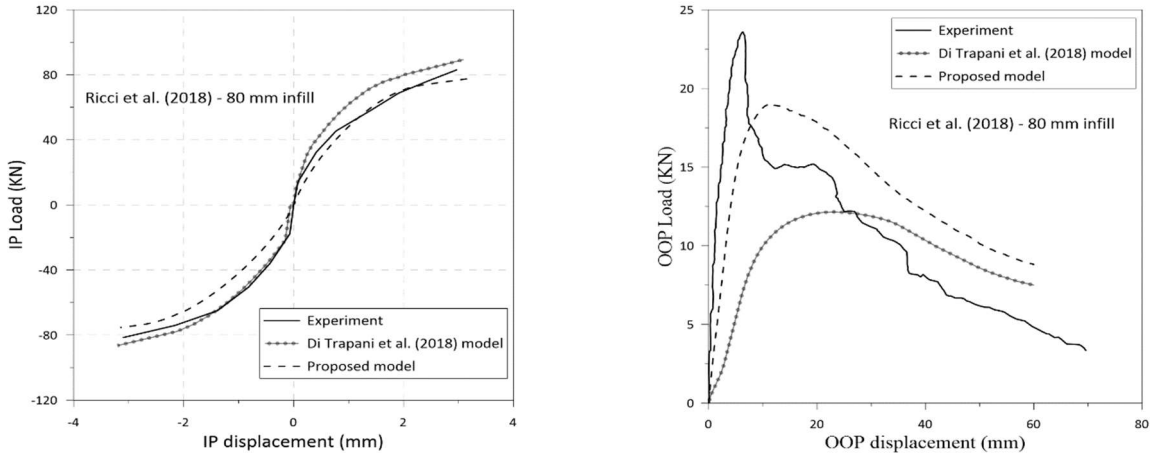

(a) (b)

279 **Fig 19** Comparison of responses for specimen #1 of Rici et al. (2018): a) IP responses; b) OOP responses

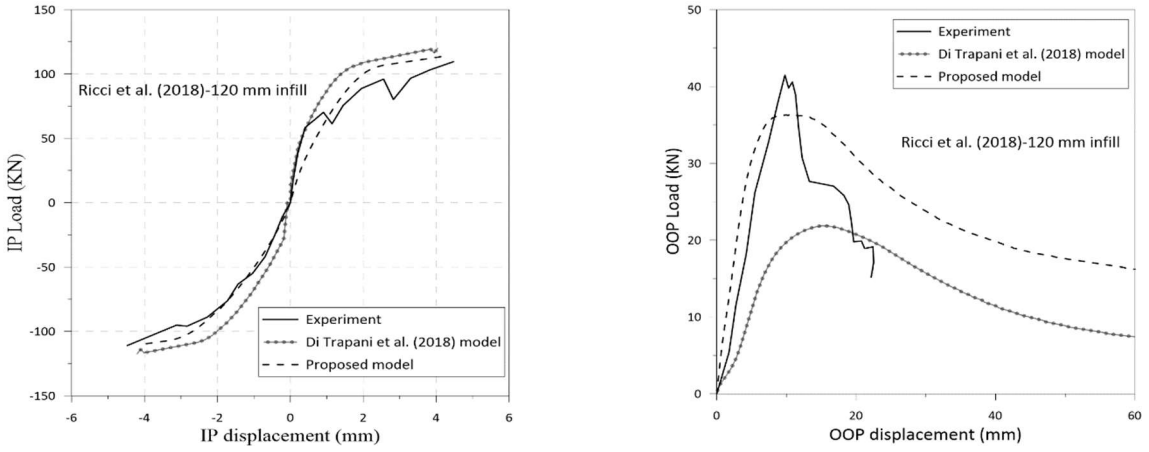

(a) (b)

280 **Fig 20** Comparison of responses for specimen #2 of Ricci et al. (2018): a) IP responses; b) OOP responses

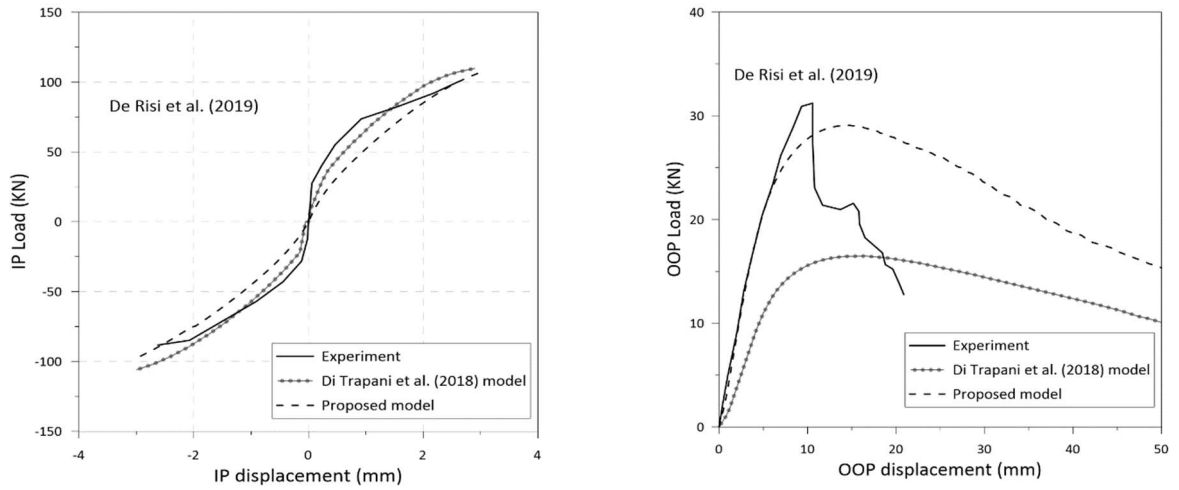

(a) (b)

281 **Fig 21** Comparison of responses for De Risi et al. (2019): a) IP responses; b) OOP responses

282 From the above figures, it can be seen that the numerical results obtained are good representation of
283 the experimental responses. Both IP and OOP responses obtained from the numerical analyses are
284 close to the experimental results. The model is able to take into account the effect of prior IP damage
285 on the OOP response. This shows the possibility of using the proposed macro element model to
286 describe the IP and OOP behavior of URM infill wall under seismic actions.

287 The numerical simulations were also performed by using the original four strut macro model of Di
288 Trapani et al. [43] using the same empirical parameters that were used for the proposed model and
289 the results are kept in the same Fig 17-21 for better comparison between the outputs from two models.
290 It can be observed that IP responses from both models are good simulations of experimental results.
291 However, regarding the OOP response, the proposed model has better capacity. This verifies that the
292 proposed modifications enable the model to capture the arching mechanism of the URM infill wall
293 under OOP load in a more reliable way.

294 Each of the diagonal, vertical and horizontal struts play effective role in OOP resistance in the model.
295 The contributions of the individual struts in the OOP resistance are shown in Fig 22. The numerical
296 results show that the resistance given by diagonal and vertical struts are higher than the horizontal
297 struts as in the case of simulation for Angel [1].

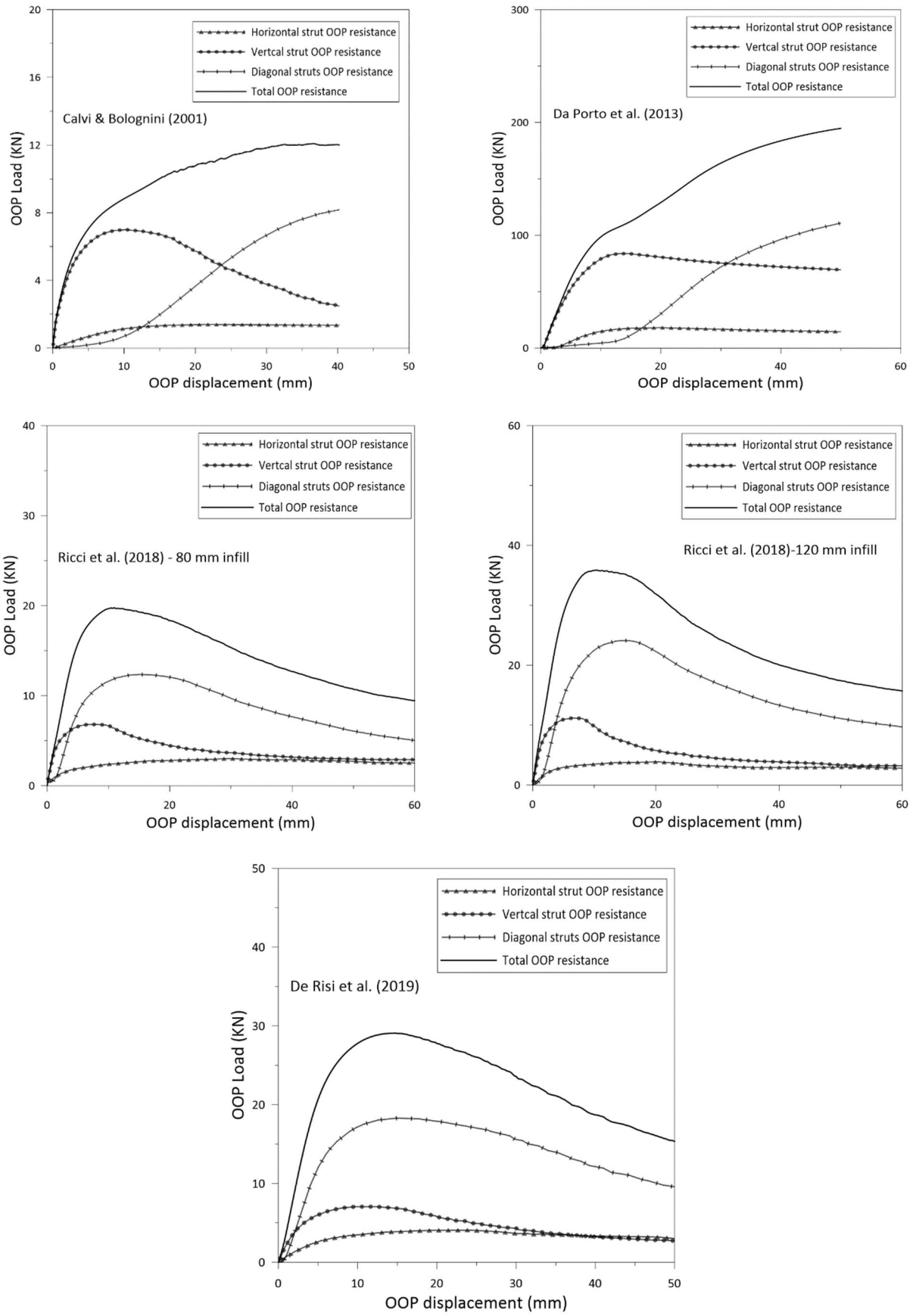

298 **Fig 22** Role of horizontal, vertical and diagonal struts in resisting the OOP load

299

4. Correlation between empirical parameters and mechanical properties of masonry

Empirical strength strain parameters are key elements for the proposed macro element model; they describe the compressive behaviour of the struts. These parameters cannot be assigned randomly for the analysis of infilled frame structures, rather they are to be selected by a standard procedure. To establish a standard relation, three parameters f_{mo}, ε_{mo} and ε_{mu} were chosen and multiple analysis were performed and subsequent optimizations were done based on the observed results. These parameters were taken based on the value of the infill wall properties i.e. the product of f_m and E_m or simply $f_m E_m$. As mentioned in the earlier section, the analysis were performed in such a way that certain degree of correlation could be established and at the same time the responses obtained were close to the experimental results. Roughly correlated parameters established for all the later experimental specimens along with those used for the validation of the proposed model using Angel [1]'s specimens are put together and plotted by a best fitting curve. The best fitting curves are represented by the following empirical equations [Eq. 10 -12]. The infill parameter (f_m E_m) and strut parameters (f_{mo}, ε_{mo}, ε_{mu}) which were finally used to establish the empirical equations are given in Table 6. The correlation between the parameters are shown by the curves in Fig 23.

$$f_{mo} = \begin{cases} 0.61 + 0.0001\, f_m\, E_m - 10^{-9}(f_m\, E_m)^2, & f_m\, E_m < 40000 \\ 3, & f_m\, E_m \geq 40000 \end{cases} \quad [10]$$

$$\varepsilon_{mo} = 4 \times 10^{-8}\, f_m\, E_m + 0.00039 \quad [11]$$

$$\varepsilon_{mu} = \begin{cases} 0.0044 + 4 \times 10^{-7}\, f_m\, E_m - 3.4 \times 10^{-12}(f_m\, E_m)^2, & f_m\, E_m < 48000 \\ 0.017, & f_m\, E_m \geq 48000 \end{cases} \quad [12]$$

Table 6 Correlation of infill properties with the empirical parameters

Experimental study		Infill properties			Strut properties		
		f_m N/mm^2	E_m N/mm^2	$f_m E_m$ N^2/mm^4	f_{mo} N/mm^2	ε_{mo}	ε_{mu}
Calvi and Bolognini (2001)	#6	1.11	1362.4	1505.452	0.77	0.00046	0.0045
Ricci et al. (2018)	#1	2.11	1169.59	2467.843	0.79	0.00052	0.0056
	#2	1.87	1355.07	2533.978	0.79	0.00054	0.0058
Da Porta et al. (2013)		2.67	2760.31	7370.028	1.4	0.00064	0.0074
De Resi et al. (2019)		3.31	2554.94	8456.86	1.5	0.00068	0.0076
Angel (1994)	S2	10.85	8046.18	87301	2.6	0.0038	0.018
Angel (1994)	S3	10.13	5212.44	52802	3.6	0.0030	0.015

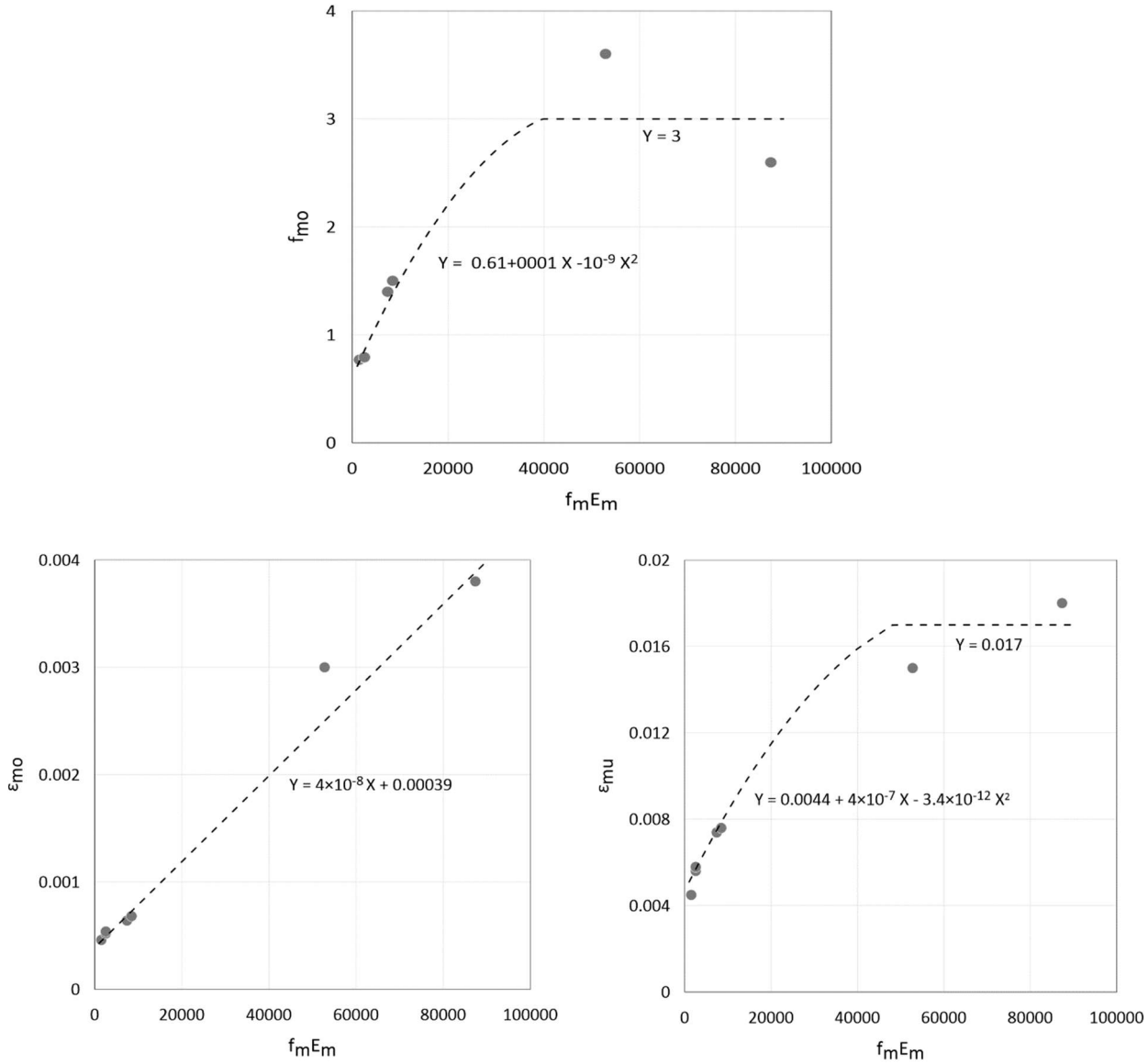

Fig 23 Relationship to obtain the empirical parameters given by Eq. 10 -12

According to the above equations, the value of f_{mo} increases with the increase in the value of f_mE_m nonlinearly up to 40000 and beyond which it becomes constant. Similar relation is also derived for the case of f_{mu} where its value increases with f_mE_m up to a value of 48000 and maintains a constant value after that point. The value of ε_{mo} increases linearly with the increase in the value of f_mE_m. The above empirical equations are established by fitting small number of data in the best possible way. The values of f_{mo} and f_{mu} in the higher range of f_mE_m are proposed to be constant after observing the results of multiple numerical simulations for Angel [1]'s specimens. It was found that the small change in the value of these two parameters do not influence the numerical response largely and they could be assigned a constant value in the very high range of actual infill property. The availability of

experimental data especially in the higher range of infill property can be more helpful to derive the conclusion. The effectiveness of the proposed equations to derive the empirical parameters required for the struts is already shown by the by numerical responses in Fig 17-21.

The Angel [1]'s specimens 2 and 3 are re-simulated using the parameters calculated according to proposed equations. The values of empirical parameters f_{m0}, ε_{mo} and ε_{mu} used for specimen 2 are 3, 0.0038 and 0.017 respectively while for the specimen 3, the corresponding values are 3.0, 0.0025 and 0.017 respectively. Fig 24 & 25 compares the numerical results obtained by using the parameters used for the validation purpose (before correlation) and the parameters according to the proposed equations (after correlation). The new results for Angel [1] are not as better as the earlier results; the OOP response is slightly weak. However, considering the simplicity of the proposed model & empirical equations and the need to represent both IP and OOP responses reliably, the numerical output can be considered as a close approximation of experimental results. The empirical equations can be further updated with the availability of the more experimental results (especially in the range of medium and high values of f_mE_m) in the future.

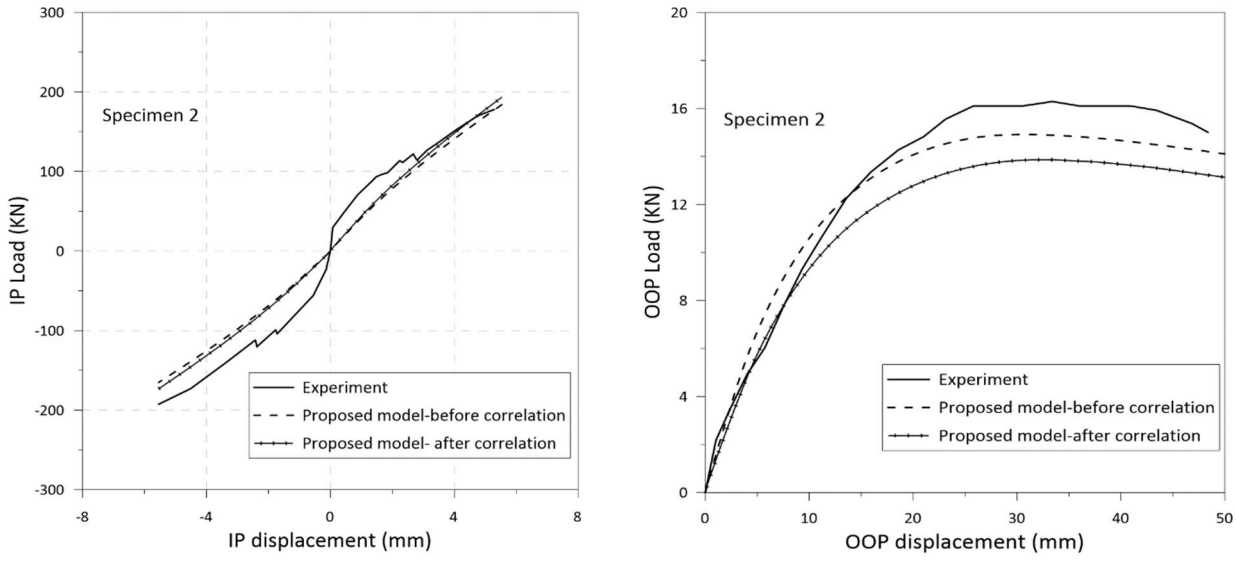

(a) (b)

Fig 24 Comparison of responses for specimen 2 of Angel (1994) before and after correlation: a) IP; b) OOP

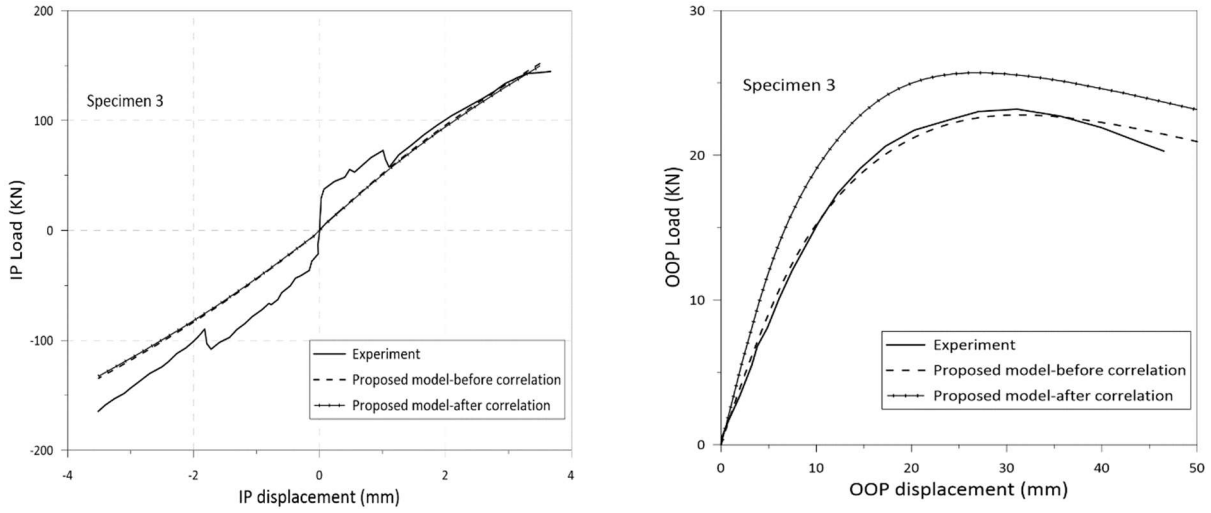

(a) (b)

346 **Fig 25** Comparison of responses for specimen 3 of Angel (1994) before and after correlation: a) IP; b) OOP

347

348 ## 5. Conclusion

349 A modified macro element model which is able to simulate the IP and OOP behaviour of URM infill
350 wall is presented in this paper. The proposed model is a modification and development over a similar
351 model having the 4 struts configuration. Struts are represented by the fiber section beam-column
352 elements and can directly take into account the arching mechanism of infill wall under the action of
353 OOP loads. The proposed model has been validated with the experimental data available in the
354 literature. The proposed modification has enhanced the capacity of the four strut macro model to
355 capture the OOP behaviour more accurately. In particular, the proposed macro model is better in
356 simulating IP and OOP responses as well as their interactions in URM infill wall under the action of
357 seismic loads. Empirical strength strain parameters are the key, in using the proposed model for the
358 analysis of infilled frame structures. Empirical equations have been proposed to determine the
359 empirical parameters required for the struts based on the actual mechanical properties of the infill
360 wall. Considering, the simplicity of the model and its effectiveness to simulate IP and OOP responses
361 as well as the interaction effect, the proposed macro model can be considered as a much needed
362 achievement in the development of macro element modeling technique.

References:

[1] Angel R. (1994). "Behavior of reinforced concrete frames with masonry infill walls." Ph.D. thesis, Univ. of Illinois, Urbana-Champaign, IL1994.

[2] Flanagan RD, and Bennet RM. Bidirectional behavior of structural clay tile infilled frames. J. Struct. Eng.1999; 10.1061/(ASCE) 0733-9445(1999)125:3(236), 236–244.

[3] Calvi GM, Bolognini D. Seismic Response of Reinforced Concrete Frames Infilled with Weakly Reinforced Masonry Panels, Journal of Earthquake Engineering 2001; 5:153-185.

[4] Anić F, Penava D, Abrahamczyk L, Sarhosis V. Computational evaluation of experimental methodologies of out-of-plane behavior of framed-walls with opening, Earthquake and Structures 2019; 16(3): 265-277.

[5] Anić F, Penava D, Varevac D, Sarhosis V. Influence of clay block masonry properties on the out-of-plane behaviour of infilled RC frames, Tehnicki Vjesnik 2019; 26(3): 831-836.

[6] Henderson R, Jones W, Burdette E, Porter M. The effect of prior out-of-plane damage on the in-plane behavior of unreinforced masonry infilled frames. In: The Fourth DOE Natural Phenomena Hazards Mitigation Conference 1993.

[7] Palieraki V, Zeris C, Vintzileou E, Adami C-E. In-plane and out-of-plane response of currently constructed masonry infills. Eng Struct. 2018; 177:103–16.

[8] Ricci P, Di Domenico M, Verderame GM. Experimental assessment of the in-plane/ out-of-plane interaction in unreinforced masonry infill walls. Eng Struct 2018;2018(173):960–78

[9] De Risi MT, Di Domenico M, Ricci P, Verderame GM, Manfredi G. Experimental investigation on the influence of the aspect ratio on the in-plane/out-of-plane interaction for masonry infills in RC frames. Eng Struct. 2019; 189:523–40.

[10] Polyakov SV. On the Interaction between Masonry Filler Walls and Enclosing Frame When Loading in the Plane of the Wall. Translation in Earthquake Engineering. Earthquake Engineering Research Institute 1960; 36–42

[11] Holmes M. Steel Frames with Brickwork and Concrete Infilling, in: Proceedings of the Institution of Civil Engineers 1961; 473–478

[12] Smith B. Lateral Stiffness of Infilled Frames. ASCE Journal of Structural Division 1962; 88, 183–199

[13] Smith BS, Carter C. A Method of Analysis for Infilled Frames, in: Proceedings of the Institution of Civil Engineers 1959; 31–48

[14] Mainstone RJ. Supplementary Note on the Stiffness and Strengths of Infilled Frames. Presented at the Building Research Station, 1974; Garston, UK.

[15] Liauw TC. An Approximate Method of Analysis for Infilled Frames with or without Opening. Building Science 1972; 7(4):233-238.

[16] Paulay T, Priestley MJN. Seismic Design of Reinforced Concrete and Masonry Buildings. Wiley, c, 1992; New York.

[17] Durrani AJ, Luo YH. Seismic Retrofit of Flat-Slab Buildings with Masonry Infills, in: NCEER Workshop on Seismic Response of Masonry Infills. National Center for Earthquake Engineering Research (NCEER), 1994; Buffalo, NY

[18] Hendry AW. Structural Masonry, II. ed., 1998; Palgrave.

[19] Al-Chaar G. Evaluating Strength and Stiffness of Unreinforced Masonry Infill Structures: Defense Technical Information Center. 2002; Fort Belvoir, VA

[20] Thiruvengadam V. On the Natural Frequencies of Infilled Frames. Earthquake Engineering & Structural Dynamics 13, 401–419.

[21] Chrysostomou CZ. Effects of Degrading Infill Walls on the Nonlinear Seismic Response of Two-Dimensional Steel Frames (PhD). Cornell University, 1991; New York, USA.

[22] Chrysostomou CZ, Gergely P, Abel JF. A Six-Strut Model for Nonlinear Dynamic Analysis of Steel Infilled Frames. International Journal of Structural Stability and Dynamics 2002; 2, 335–353

[23] El-Dakhakhni WW. Experimental and Analytical Seismic Evaluation of Concrete Masonry-Infilled Steel Frames Retrofitted Using GFRP Laminates (PhD). Drexel University, 2002; Philadelphia, USA.

[24] El-Dakhakhni WW, Elgaaly M, Hamid AA. Three-Strut Model for Concrete Masonry-Infilled Steel Frames. Journal of Structural Engineering, 2003; 129, 177–185.

[25] Crisafulli FJ. Seismic Behaviour of Reinforced Concrete Structures with Masonry Infills (PhD). University of Canterbury, 1997; New Zealand.

[26] Crisafulli FJ, Carr AJ. Proposed Macro-Model For The Analysis Of Infilled Frame Structures. Bulletin of New Zealand National Society for Earthquake Engineering, 2007; 40, 9

[27] Papia M, Cavaleri L, Fossetti M. Infilled frames: Developments in the evaluation of the stiffening effect of infills. Struct. Eng. Mech., 2003; 16(6), 675–693

[28] Asteris PG, Cavaleri L, Di Trapani F, Sarhosis V. A macro-modelling approach for the analysis of infilled frame structures considering the effects of openings and vertical loads. Struct. Infrastruct. Eng., 2015; 10.1080/15732479.2015.1030761, 12(5), 551–566

[29] Panagiotakos TB, Fardis, MN. Seismic response of infilled RC frames structures. Proc., XXI World Conf. of Earthquake Engineering, 1996; Acapulco, Mexico

[30] Žarni´c R, Gostič S. Masonry infilled frames as an effective structural subassemblage. Seismic design methodologies for the next generation of codes, 1997; P. Fajfar and H. Krawinkler, eds., A.A. Balkema, Rotterdam, Netherlands, 335–346.

[31] Dolšek M, Fajfar P. Simplified non-linear seismic analysis of infilled reinforced concrete frames. Earthq Eng Struct Dyn, 2005; 34:49–66.

[32] Madan A, Reinhorn AM, Mander JB, Valles RE. "Modeling of masonry infill panels for structural analysis." J. Struct. Eng., 1997; 10.1061/(ASCE)0733 9445(1997)123:10(1295), 1295 1302.

[33] Cavaleri L, Fossetti M, Papia M. Infilled frames: Developments in the evaluation of cyclic behavior under lateral loads." Struct. Eng. Mech. 2005, 21(4), 469–494.

[34] Rodrigues H, Varum H, Costa A. Simplified macro-model for infill masonry panels. Journal of Earthquake Engineering 2010; 14:390–416

[35] Cavaleri L, Di Trapani F. Cyclic response of masonry infilled RC frames: Experimental results and simplified modeling. Soil Dynamics and Earthquake Engineering 2014; 65: 224-42.

[36] Hashemi SA, Mosalam KM. Seismic evaluation of reinforced concrete buildings including effects of infill masonry walls. PEER 2007/100 2007; Univ. of California, Berkeley, CA.

[37] Kadysiewski S, Mosalam KM. Modeling of unreinforced masonry infill walls considering in-plane and out-of-plane interaction. PEER 2008/102 2009; Univ. of California, Berkeley, CA.

[38] Mosalam KM, Günay S. "Progressive collapse analysis of RC frames with URM infill walls considering in-plane/out-of-plane interaction." Earthquake Spectra 2015; 31(2), 921–943.

[39] McKenna F, Fenves G, Scott M, Jeremic B. Open System for Earthquake Engineering Simulation (OpenSees). 2000, Berkeley.

[40] Furtado A, Rodrigues H, Arede A, Varum H. Simplified macro-model for infill masonry walls considering the out-of-plane behavior. J Earthq Eng Struct Dyn. 2015; 45:507–524

[41] Al Hanoun HM, Abrahamczyk L, Schwarz J. Macromodeling of in- and out-of-plane behavior of unreinforced masonry infill walls. Bull Earthq Eng. 2018;

[42] SAP2000 (2005) Linear and nonlinear static and dynamic analysis and design of three-dimensional structures, vol 10. Computers and Structures, Inc., 2010; Berkeley

[43] Di Trapani F, Shing PB, Cavaleri L. A macro-element model for in-plane and out-of-plane responses of masonry infills in frame structures. J. Struct. Eng. 2018; 144 (2): 04017198.

[44] Asteris PG, Cavaleri L, Di Trapani F, Tsaris AK. Numerical modelling of out-of-plane response of infilled frames: State of the art and future challenges for the equivalent strut macromodels. Eng Struct. 2017; 132:110–22.

[45] Di Trapani F, Bertagnoli G, Ferrotto MF, Gino D. Empirical Equations for the Direct Definition of Stress–Strain Laws for Fiber-Section-Based Macro-modeling of Infilled Frames. J Eng Mech. 2018;144(11):17.

[46] Kent DC, Park R. Flexural members with confined concrete. J. Struct Eng. 1971. 97(ST7), 1969–1990.

[47] Da Porto F, Guidi G, Benetta MD, Verlato N. Combined In-Plane/Out-of-Plane Experimental Behaviour of Reinforced and Strengthened Infill Masonry Walls. The Masonry Society, ed. 12th Canadian Masonry Symposium 2013;12.

[48] Pereira MFP, Pereira MFN, Ferreira JED, Lourenço PB. Behaviour of masonry infill panels in RC frames subjected to in plane and out of plane loads. In: 7th international conference on analytical models and new concepts in concrete and masonry structures; 2011.

[49] Hak S, Morandi P, Magenes G. Out-of-plane experimental response of strong masonry infills. In: 2nd European conference on earthquake engineering and seismology; 2014

[50] Furtado A, Rodrigues H, Arêde A, Varum H. Experimental evaluation of out-of-plane capacity of masonry infill walls. Eng Struct 2016;111:48–63.